# Linear Pattern Correction Technique for Compensating the Effects of Mutual Coupling and Deformation in Wedge-Shaped Conformal Antenna Arrays

## Adnan Tariq, Shahid Khattak, Hina Munsif, Sohail Razzaq, and Irfanullah[*]

Department of Electrical and Computer Engineering
COMSATS University Islamabad, Abbottabad Campus, Pakistan
*eengr@cuiatd.edu.pk

***Abstract*** ─ In this paper, the effects of mutual coupling and antenna surface deformity in a conformal wedge-shaped antenna array are compensated using a linear pattern correction technique. The problem is formulated to reduce the absolute distance between the actual (simulated) and the desired radiation patterns and to allow for null positioning control. The individual field patterns for the antenna elements are deformed due to changes in mutual coupling and the conformal surface. The deformed patterns of the individual antennas for specific bend angles are stored as lookup tables and interpolated to get the desired radiation pattern at any arbitrary bend-angle. The problem is linearly and quadratically constrained at the null points and performance compared with unconstrained optimization. The proposed solution for diminishing the effect of mutual coupling and surface deformity is independent of main lobe direction, type of individual antenna, array geometry, and spacing between antenna elements. The closed-form results are validated through Computer Simulation Technology (CST) for the wedge-shaped deformed dipole antenna array. The results for the proposed scheme are also assessed with the traditional Open Circuit Voltage Method (OCVM) and show superior compensation for deformity and the mutual coupling effects in conformal beam-forming arrays in terms of main beam direction, position and depth of nulls.

***Index Terms*** ─ Aerial platform, conformal antenna array, interpolation of patterns, least square estimation, mutual coupling compensation, radiation pattern correction.

## I. INTRODUCTION

Modern 5G networks comprise heterogeneous systems overseeing massive data transfer capacities and with the high frequency of access points. In order to make these access points less noticeable to the natural eye, they would be required to conform in shape to everyday objects around us [1]. A conformal antenna array can be defined as an array that follows the surface of objects whose shape is defined by considerations other than electromagnetic [2].

Besides 5G wireless massive Multiple Input Multiple Output (MIMO) systems, spatial filtering achieved by conformal antenna array also has applications in radar, and target tracking [3]. Additionally, conformal antenna arrays can be used to replace numerous antennas protuberant from the surface of modern aircraft which are used for navigation, radar altimeter, instrument landing systems and various communication systems [1], [4]-[6] causing considerable mechanical strain and increased fuel ingestion. The need for conformal reception apparatuses is much higher for the large-sized openings that are required for capacities like military airborne observation radars and satellite correspondence [2].

The surfaces, on which the conformal antennas are mounted, may not be sturdy structures and are susceptible to physical deformation because of natural changes. This flexing of surfaces will make the original positions of the antenna component change, resulting in changes in steering vector and Mutual Coupling (MC) among them and producing the radiation pattern conduct entirely unreliable [7], [8]. The subsequent pattern alteration may shift the location of the main beam and loss of null points which minimizes the expected gain of the antenna array and may render any Signal-Not-of-Interest (SNOI) avoidance through the shaping of the radiation pattern. Researchers are, therefore, focusing on compensation techniques in order to accurately recover the beam pattern and directivity of the antenna array to direct the nulls and the main beam to any wanted direction irrespective of the extent of the distortion of the conformal surface. Through defined employment of the broadside pattern and the nulls, with no power-driven movement of the antenna elements [2], high signal to noise plus interference ratio (SNIR) is attained.

The impact of MC on the wire antenna (monopole antenna, dipole antenna etc.) in an array can be demonstrated through variations in their input impedances. This idea was first introduced by Gupta in [9], where an impedance matrix was utilized to relieve the impact of MC in a planar array of dipole antennas. In [10], [11], this method was used for Direction of Arrival

(DOA) signal estimation and adaptive nulling of interference. Hui in [11] modelled the MC using impedance matrix based on estimated current distribution and it was shown that the new method for modelling MC performs better in terms of DOA estimation. Notwithstanding, the impedance matrix was assessed under the supposition that the antenna will not radiate while open-circuited in the Open-Circuit Voltage Method (OCVM), which limits this technique to wire antenna elements only.

Another technique called Linear Pattern Correction Method (LPCM) reduces the impacts of MC in antenna arrays through pattern adjustment by limiting the Mean Square Error (MSE) between the wanted and actual patterns [10]-[16]. The outcomes show that the complex excitations for array component assessed utilizing the LPCM are more powerful in alleviating the impacts of MC than OCVM [14],[19]. Since unconstrained LPCM attempts to decrease the MSE between actual and wanted patterns, its effect is less pronounced on patterns alongside directions where signal quality is low, i.e., along with null points.

In [17], the genetic algorithm is used to determine the optimum antenna element excitation for a conformal array. In [11], a framework for radiation pattern synthesis is developed using convex optimization theory in order to optimize dual-polarized conformal arrays. However, both these techniques exhibit higher complexity than LPCM and would bring only marginal performance gains.

In [3], [17], the phase compensation procedure is deployed to recover the desired antenna array pattern for conformal antennas after incorporating the surface deformity and MC effect. In this method, the projection technique has been utilized to ascertain the measure of phase shift presented by every component in an array to arrive at the reference plane, which is then consolidated in the excitations to recover the ideal pattern. No exertion has been done to recover the nulls in this method and there is no control on the arrangement of sidelobes. In [15], the LPCM is implemented to deformed conformal antenna arrays utilizing the impedance matrix of the distorted antenna array acquired from [7]. Direct imperatives are additionally incorporated at the null points so as to govern their position and depth. This model when tried in CST for bigger deformations gives insufficient compensation. The radiation pattern compensation for conformal beamforming array with precise control at the desired direction is, therefore, an open research area and the focus of this paper.

In the introduced work, a practical procedure is created and tested for absolutely controlling the array pattern of deformed conformal antennas through constrained optimization of LPCM. Both the linear and quadratic constraints have been considered. The effect of varying mutual coupling due to deformation is compensated using pre-calculated separately evaluated antenna patterns at various bend angles. The technique is independent of inter-element spacing and antenna element type and has been tested successfully for different deformation angles through interpolation of patterns and for different main beam directions. Even though the strategy is just tested here for wedge-shaped surfaces, it is independent of the surface geometry as long as the position and direction of the individual antenna component are accurately characterized.

The remainder of the paper is organized as follows: In Section II, the problem is formulated. In Section III, the proposed solution for deformity and MC reduction is discussed. Section IV and V the results and their detailed analysis are presented. Section VI finally concludes the paper.

*Notation:* All matrices are shown in boldface capital letters (**E, A, V, etc.**), vectors are represented by boldface small-case letters (**w, b etc.**), while all the scaler quantities are represented as normal letters. $|\cdot|$ represents the absolute value and $\|\cdot\|$ represents the Euclidean norm.

## II. PROBLEM FORMULATION

The physical layout of an $N$-dipole conformal antenna array mounted on a wedge shape surface, formed along the XZ-plane, is shown in Fig. 1. The antenna elements are equally divided on either side of the wedge with equal inter-element spacing $d$. The individual dipoles are oriented along Y-axis in order to increase the MC between them so that the effectiveness of the proposed algorithm can be better demonstrated. Bend angle $\Upsilon$, between the surface of the wedge and X-axis, can be varied, resulting in pattern distortions due to change in antenna locations and orientations. This also affects the relative distances between the antenna elements and changes the MC.
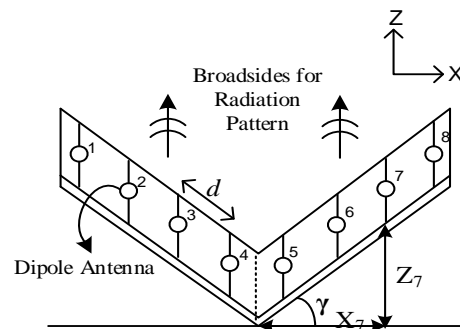


Fig. 1. A deformed wedge shape antenna array in XZ-plane with eight dipole antennas and a bend angle $\Upsilon$.

The two planar wedge surfaces are considered inflexible and the deformity only occurs as the bend angle changes. The location of an individual element in antenna array along X and Z directions is measured by

the following equations respectively,

$$x_n(d, \Upsilon) = \left(-(N-1)\frac{d}{2} + (n-1)d\right)\cos(\Upsilon), \quad (1)$$

$$z_n(d, \Upsilon) = \left|\left(-(N-1)\frac{d}{2} + (n-1)d\right)\right|\sin(\Upsilon),$$

where $n = 1, \cdots, N$. The position of all the antennas along the Y direction is assumed fixed. A three-dimensional steering matrix is formed $\mathbf{V} \in \mathbb{C}^{[M \times J \times N]}$, with each element $v(m, j, n)$ given by:

$$v(\theta_m, \phi_j, n)$$
$$= e^{-j\frac{2\pi}{\lambda}[x_n(sin\theta_m cos\phi_j) + y_n(sin\theta_m sin\phi_j) + z_n(cos\theta_m)]}, \quad (2)$$

where $x_n, y_n$ and $z_n$ is the location of the $n^{th}$ element in the array, $\theta_m \in \{\theta_1, \ldots, \theta_M\}$ is the elevation steering angle and $\phi_j \in \{\phi_1, \ldots, \phi_J\}$ is the azimuth steering angle. $M$ and $J$ are the total numbers of elevation and azimuth angle points respectively.

Individual element patterns for dipole antennas are concatenated to form a three-dimensional matrix $\mathbf{P}$ such that $\mathbf{P} \in \mathbb{C}^{[M \times N \times J]}$. The Array Pattern matrix $\mathbf{A}$ is given as the element-wise product of matrix $\mathbf{V}$ and $\mathbf{P}$, i.e., $\mathbf{A} = \mathbf{V} \odot \mathbf{P}$. The field pattern $\mathbf{E}$ at any arbitrary angle $\theta_m$ and $\phi_j$ can be calculated as:

$$\mathbf{E}(\theta_m, \phi_j) = \mathbf{A}(\theta_m, \phi_j)\,\mathbf{w} \quad (3)$$

where $\mathbf{w}$ represent the complex excitations to the antenna elements. For succeeding analysis, $\phi_j$ has been presumed static and the resulting patterns have been observed for the elevation angle $\theta$ only.

When the bend angle $\Upsilon$ changes due to external conditions, the whole array pattern distorts due to changes in MC and steering matrix $\mathbf{V}$. The problem is to adapt the weights $\mathbf{w}$ with changes in $\Upsilon$ so as to compensate for any radiation pattern errors due to distortion in the shape of the conformal surface.

## III. PROPOSED SOLUTION

### A. Procedure for compensation

The flowchart presented in Fig. 2 predicts the approach implemented for deformity compensation and reduction of the MC effect. Here, the deformity is defined as changes in the position of individual antennas elements as the $\Upsilon$ changes. A single dipole antenna is designed in CST Studio Suite and desired array pattern $\mathbf{A}_{des} \in \mathbb{C}^{M \times N}$ is shaped by the element-wise product of the concatenated isolated pattern of individual element (taken from CST Studio Suite) with the steering matrix ($V$). The initial excitations $\mathbf{w}_i$ given to each array element are extracted by optimizing the pattern of the antenna that minimizes $\mathbf{w}_i$ while having the main beam and null points at the desired positions. The optimization problem is written as:

$$\min_{\mathbf{w}_i} \sum_i \|\mathbf{E}_{des}(\theta_{SB})\|,$$
$$\text{s.t.} \quad \mathbf{E}_{des}(\theta_{tar}) = 1, \quad (4)$$
$$\mathbf{E}_{des}(\theta_{null}) \le \epsilon,$$

where $\theta_{tar}$ and $\theta_{null}$ are the target and null directions respectively and $\epsilon$ is an arbitrary null depth. $\mathbf{E}_{des} = \mathbf{A}_{des}\mathbf{w}_i$ is the required field pattern. The constraints here ensure that null point positions are precisely defined, and nulls are of sufficient depth to test between the algorithms. The compensation algorithms require individual antenna patterns $\mathbf{P}_{def}$ incorporating the effect of deformation and MC, the desired pattern of array and location of the radiating antenna elements. It calculates the compensated weights $\mathbf{w}_c$, which mitigates the effect of deformity and MC. The compensated field pattern is given by $\mathbf{E}_c$.

### B. OCVM and LPCM

OCVM is the most commonly cited technique for compensation of MC and deformity effect in conformal arrays with wired antennas. In OCVM, dimensionless normalized impedance matrix $\mathbf{Z}_c$ is used to compensate for the MC by taking the product of its inverse $\mathbf{Z}_c^{-1}$ and the open-circuited voltages $\mathbf{v}_{oc}$ as the terminal voltage $\mathbf{v}_T = \mathbf{Z}_c^{-1}\mathbf{v}_{oc}$ [9]. The closed-form expression for the impedances for wired antennas is obtained by assuming the antenna array as an $N-$port network as explained in [13]. For more complex antenna elements, the moments method is used for obtaining $\mathbf{Z}_c$. However, due to non-zero antenna current under open-circuit, $\mathbf{Z}_c$ fails to accurately model the antenna behaviour. This method, therefore, suffers from considerable error as the nulls are not only filled up but their positions are also shifted. For conformal antenna arrays, the situation gets even worse as the effect of small approximation errors for individual antennas is compounded as their patterns are combined with less than optimal phases and amplitudes. As a result, the final array pattern looks very different from the desired one.
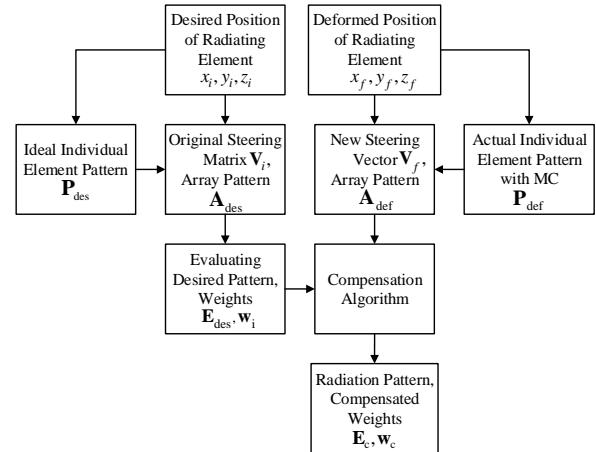


Fig. 2. The procedure adopted for compensating the effect of MC and surface deformity in conformal antenna arrays.

A more accurate procedure for alleviating the MC

and deformation impact from array pattern is the Linear Pattern Correction Method (LPCM) which attempts to limit the Euclidean separation among actual and ($\mathbf{E}_{\text{def}}$) and desired ($\mathbf{E}_{\text{des}}$) field patterns. It aims to reduce the Mean Square Error (MSE) between the simulated deformed and desired APs as shown in the equation,

$$\min_{\mathbf{w}_c} \sum_\theta \|\mathbf{A}_{\text{def}}\mathbf{w}_c - \mathbf{A}_{\text{des}}\mathbf{w}_i\|^2. \tag{5}$$

In [14], it has been observed that the distorted pattern is recovered through matrix $\mathbf{K}$ obtained as:

$$\mathbf{K} = (\mathbf{A}_{\text{def}})^\dagger \mathbf{A}_{\text{des}},$$
$$\mathbf{w}_c = \mathbf{K}.\,\mathbf{w}_i, \tag{6}$$
$$\mathbf{E}_c = \mathbf{A}_{\text{def}}\,\mathbf{w}_c,$$

where $\dagger$ indicates the pseudoinverse and is defined as $(\mathbf{A}_{\text{def}})^\dagger = \mathbf{A}_{\text{def}}^H(\mathbf{A}_{\text{def}}\mathbf{A}_{\text{def}}^H)^{-1}$. Here $\mathbf{A}_{\text{def}} \in \mathbb{C}^{M \times N}$ is the matrix containing defomed patterns of an individual element in array and $\mathbf{E}_c \in \mathbb{C}^{M \times 1}$ is the radiation pattern of corrected element patterns. The vector $\mathbf{w}_i$ contain the initial excitations used to obtain desired array pattern, and $\mathbf{w}_c$ contain the recovered excitations which compensate for MC and antenna deformity. It is suggested to use the individual antenna patterns obtained from CST at required bend angle $\Upsilon$ values which are to be utilized as a lookup table for pattern compensation. As LPCM decreases the MSE between the patterns giving the same weight to all angles, the comparative error between the recovered pattern and desired one is much smaller at the main beam than the ones at the nulls. This is evident in the electric field radiation pattern plotted in dBs, where the nulls can be seen as shifted and the algorithm is shown to have little control over the depth of the nulls.

## C. Linear and quadratic constrained LPCM

In order to precisely control the null depth and position, LPCM is modified by introducing either linear or quadratic constraints at those points on the pattern that needs to be recovered precisely.

In Linearly Constrained (LC) LPCM, the Euclidean distance between the simulated deformed pattern $\mathbf{E}_{\text{def}}$ and desired pattern $\mathbf{E}_{\text{des}}$ is minimized while constraining the pattern at some points (either null points or the peak sidelobe points) to find the compensated weights $\mathbf{w}_c$. The LC-LPCM optimization problem is written as:

$$\min_{\mathbf{w}_c} \sum_\theta \|\mathbf{A}_{\text{def}}\mathbf{w}_c - \mathbf{AP}_{\text{des}}\mathbf{w}_i\|^2, \tag{7}$$
$$\text{s. t.} \quad \mathbf{A}_c\mathbf{w}_c = \mathbf{b},$$

where

$$\mathbf{AP}_c = [\mathbf{A}_{\text{def}}(\theta_1), \mathbf{A}_{\text{def}}(\theta_2) \cdots \mathbf{A}_{\text{def}}(\theta_q)]^T,$$
$$\mathbf{E}_{\text{des}} = \mathbf{A}_{\text{des}}\mathbf{w}_i, \tag{8}$$
$$\mathbf{b} = [\mathbf{E}_{\text{des}}(\theta_1), \mathbf{E}_{\text{des}}(\theta_2), \cdots, \mathbf{E}_{\text{des}}(\theta_q)]^T.$$

Here, $\mathbf{A}_c \in \mathbb{C}^{q \times N}$ is a matrix containing the $q$ constraint vectors at desired constrained angles in the simulated deformed individual element pattern matrix and $\mathbf{b} \in \mathbb{C}^{q \times 1}$ is a vector of $q$ constraint points on desired array

pattern. To find out the solution for (7) the objective function is expanded as:

$$\|\mathbf{A}_{\text{def}}\mathbf{w}_c - \mathbf{E}_{\text{des}}\|^2 = \mathbf{w}_c^H \mathbf{A}_{\text{def}}^H \mathbf{A}_{\text{def}}\mathbf{w}_c -$$
$$\mathbf{w}_c^H \mathbf{A}_{\text{def}}^H \mathbf{E}_{\text{des}} - \mathbf{E}_{\text{des}}^H \mathbf{A}_{\text{def}}\mathbf{w}_c + \tag{9}$$
$$\mathbf{E}_{\text{des}}^H \mathbf{E}_{\text{des}}.$$

The Lagrangian of (7) is formed by:

$$\mathscr{L}(\mathbf{w}_c, \mu) = \mathbf{w}_c^H \mathbf{A}_{\text{def}}^H \mathbf{A}_{\text{def}}\mathbf{w}_c - \mathbf{w}_c^H \mathbf{A}_{\text{def}}^H \mathbf{F}_{\text{des}} -$$
$$\mathbf{A}_{\text{def}}\mathbf{w}_c + \mathbf{E}_{\text{des}}^H \mathbf{E}_{\text{des}} + \mu(\mathbf{A}_c\mathbf{w}_c - \mathbf{b}), \tag{10}$$

where $\mu$ is the Lagrangian multiplier.

The closed-form solution for the above optimization problem is found by solving Karush-Kuhn-Tucker (KKT) conditions [18]. which are given as:

1. Primal Constraint: $\mathbf{A}_c\mathbf{w}_c - \mathbf{b} = 0$.
2. Dual Constraint: $\mu \geq 0$.
3. Complementary slackness: $\mu(\mathbf{A}_c\mathbf{w}_c - \mathbf{b}) = 0$.
4. The gradient of Lagrangian with respect to $\mathbf{w}_c$ vanishes:

$$\frac{d}{d\mathbf{w}_c}\mathscr{L}(\mathbf{w}_c, \mu) = 0 \tag{11}$$
$$2\mathbf{w}_c^H \mathbf{A}_{\text{def}}^H \mathbf{A}_{\text{def}} - 2\mathbf{E}_{\text{des}}^H \mathbf{A}_{\text{def}} + \mu\mathbf{A}_c = 0.$$

Rewriting third and fourth KKT conditions in matrix form give:

$$\begin{bmatrix} 2\mathbf{A}_{\text{def}}^H \mathbf{A}_{\text{def}} & \mathbf{A}_c \\ \mathbf{A}_c & 0 \end{bmatrix} \begin{bmatrix} \mathbf{w}_c \\ \mu \end{bmatrix} = \begin{bmatrix} 2\mathbf{E}_{\text{des}}^H \mathbf{A}_{\text{def}} \\ \mathbf{b} \end{bmatrix}. \tag{12}$$

The above system of linear equations is solved for $\mathbf{w}_c$ as:

$$\mathbf{w}_c = \mathbf{A}_c{}^\dagger \mathbf{b}. \tag{13}$$

The linear constraints reduce the search space so that the solution satisfying the constraint is the only possible solution. Consequently, the compensated pattern performs well at the null points (constraint points) but does not care for the rest of the radiation pattern. As a result, a higher side-lobe level at the edges, away from the constraint points, can be observed. The error performance of LC-LPCM, however, improves with increasing the number of constraints chosen at the point evenly spread over the radiation pattern. However, there is an upper limit on the maximum number of constraint points $q \leq N$.

The problem is therefore modified to Quadratically Constrained Quadratic Programming (QCQP), which is given as:

$$\min. \sum_\theta \|\mathbf{A}_{\text{def}}\mathbf{w}_c - \mathbf{A}_{\text{des}}\mathbf{w}_i\|^2, \tag{14}$$
$$\text{s. t.} \quad |\mathbf{A}_c\mathbf{w}_c - \mathbf{b}|^2 \leq \beta,$$

here $0 \leq \beta \leq 1$ is a constraining factor, lower the value of $\beta$ smaller the search space. Since closed form solution of QCQP do not exist, the Newton-Raphson method is used to solve for the above optimization problem. Quadratic constraint allows a good compromise, enabling the corrected pattern to follow the desired pattern more closely while at the same time ensuring that the desired null depths are achieved.

**D. Using LUTs to reduce complexity and storage cost**

In order to deal with the difficulty of evaluating the pattern of every element at different bend positions, lookup tables (LUTs) are used in computations in which these patterns are pre-calculated. Lookup table stores the patterns of each antenna element at all the combination of angles $\phi$ and $\theta$, as well as for different bend angles $\Upsilon$. The Electric field pattern illustrated in Fig. 3 changes with different bend angle $\Upsilon$ for the first array element.

Clearly, at any angle $(\theta)$, the behaviour changes regularly with $\Upsilon$ and in-between values can be evaluated with interpolation. Different combinations of $\Delta\Upsilon$ spacing and interpolation schemes are experimented with. It is found that the results generated with $\Delta\Upsilon = 5^o$ using cubic interpolation is reasonably accurate. The significant expense of figuring the individual array element pattern in the presence of MC and the effect of deformation occurred could be avoided by storing the simulated deformed pattern in LUTs for selected bend angles. The patterns at the rest of the flex angles can be accurately found through interpolation. Moreover, due to the geometric symmetry of the wedge-shaped conformal antennas only half of the patterns of the radiating element are required to be stored because in wedge shape the patterns of the elements are the flipped version of one another.
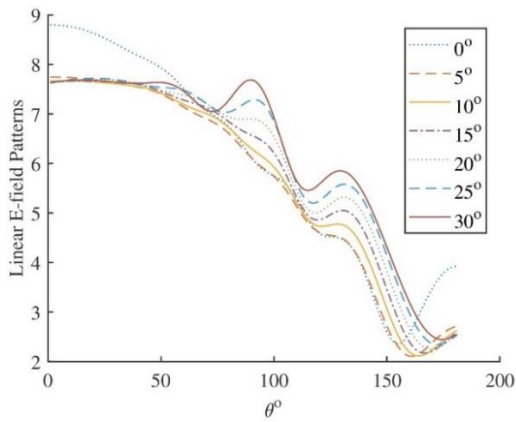


Fig. 3. Electric field pattern magnitude at different bend angles for the leftmost ($1^{st}$) array element in an 8 element wedge-shaped array at an inter-element spacing of 0.3λ.

## IV. RESULTS AND DISCUSSIONS

Eight element dipole antenna arrays have been used for simulation and analysis purposes. Inter-element spacing is kept at 0.3λ, so that the effect of MC is pronounced and the effectiveness of the proposed algorithm in mitigating it can be clearly demonstrated. 3D EM analysis software (CST) is used for verification of the results. All the radiation patterns, such as desired, deformed coupled and the compensated one, are first evaluated in MATLAB and then validated through CST. Two types of patterns have been recovered: a broadside

pattern having nulls at 30º and -30º and one with a steered the main beam towards 30º with nulls at 0º and 60º.

## A. OCVM and unconstrained LPCM compensation

In Fig. 4 OCVM and unconstrained LPCM (UC-LPCM) compensation results are shown when an 8-element linear dipole array is deformed at 15º and 30º bend-angles. The desired field pattern as shown in Figs. 4 (a) and 4 (b) is the optimized one for the linear array minimizing the sidelobe level.
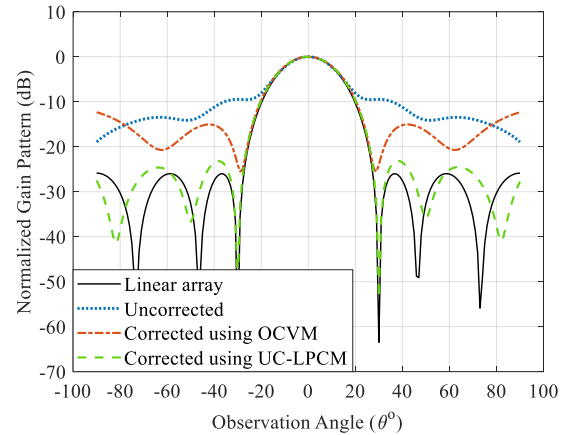


(a)
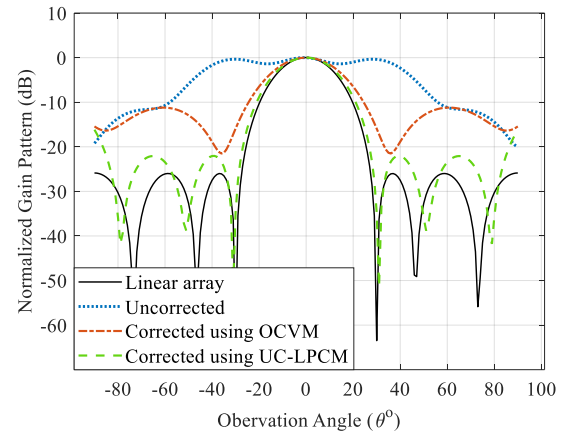


(b)

Fig. 4. OCVM and UC-LPCM compensation with the main beam at broadside for wedge shape dipole array at bend angles: (a) 15º and (b) 30º.

In OCVM, an impedance matrix is employed to find weights for deformed CBA for its pattern to approach the desired pattern. One can see in Fig. 4 (b) that OCVM is not very effective in compensating for deformation and the MC effect. In fact, at greater deformation, the impedance matrix fails to model the effect of these impairments and the compensated pattern is very different from the desired one. On the other hand, the pattern recovery is very good when using the UC-LPCM method for both small and medium deformation. The only

drawback is that the null positions have shifted by a few degrees and its depth is also gone up to around -40dB as against -60dB obtained for the desired pattern. Since UC-LPCM assigns the same weight to errors at all the angles, greater accuracy is exhibited at the peak values in the log domain representation. It is, therefore, evident from Fig. 4 that the peak to null power ratio of the compensated radiation pattern has been greatly compromised.

In Fig. 5, the results are presented for OCVM and LPCM compensation, however, the main beam is now shifted toward 30º. A wedge-shaped array is again flexed at 15º and 30º in Fig. 5 (a) and Fig. 5 (b) respectively.



(a)



(b)
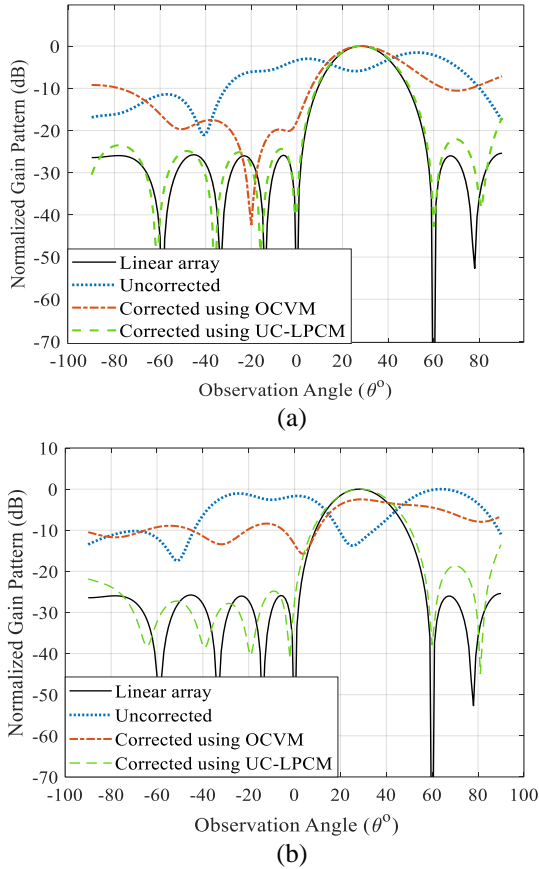
Fig. 5. OCVM and UC-LPCM compensation with the main beam centred at 30º for wedge shape dipole array at bend angles: (a) 15º and (b) 30º.

When the main beam is shifted from broadside to any other angle, OCVM fails completely to recover the pattern. It is evident that the nulls are completely lost and the sidelobe levels are higher than -10dB. The results indicate that the changed current distribution due to MC and deformation cannot be accurately modelled by the impedance matrix. The results improve considerably for unconstrained LPCM with the sidelobes dropping below -20dB. However, little control is exhibited on the

position and depth of the null points.

The results of Figs. 4 and 5 shows that OCVM has limitations for pattern recovery of severely deformed wedge antennas. While the performance is bad along the broadside, it becomes worse when the main beam is steered away from it. On the other hand, UC-LPCM gives good pattern recovery for both broadside and the steered main beam, with good sidelobe suppression. The null position and its depth, however, is greatly compromised ( >-40dB ) for the steered main beam.

## B. Linear and quadratically constrained LPCM

The algorithm works as long as the number of constraint points is less than the size of the array. To have a better trade-off between side-lobe level and nulls depth QC-LPCM results are presented, which shows the good recovery of constrained points as well as a lower side-lobe level. The search space for QC-LPCM is reduced to a hyperplane defined by the constraints. This results in a solution that gives a better trade-off between the null point recovery and the side-lobe levels.
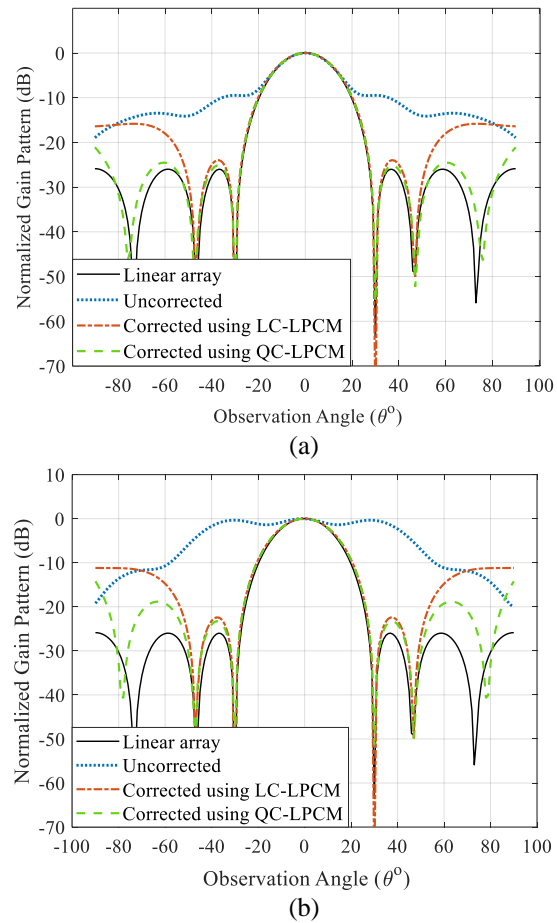


(a)



(b)

Fig. 6. LC-LPCM and QC-LPCM compensation with the main beam at broadside for wedge shape dipole array at bend angles: (a) 15º and (b) 30º.
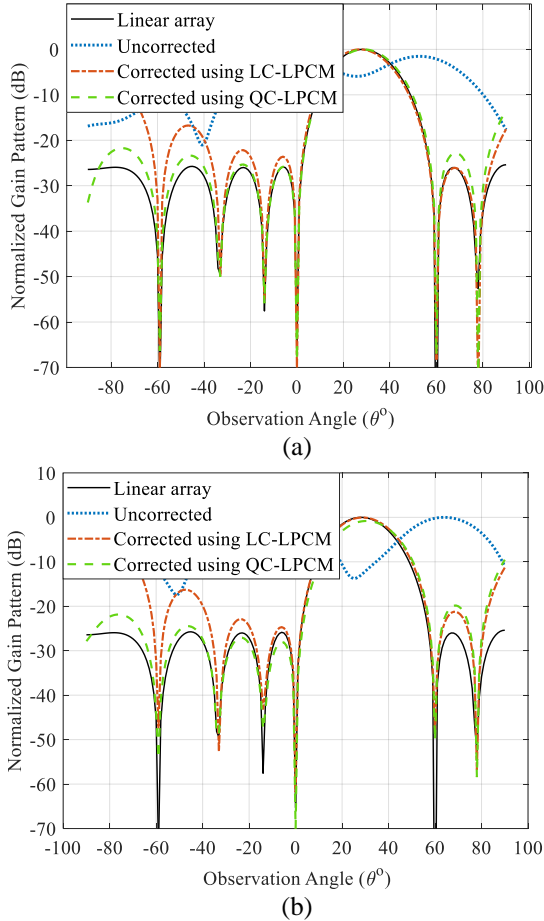
Fig. 7. LC-LPCM and QC-LPCM compensation with the main beam centred at 30° for wedge shape dipole array at bend angles: (a) 15° and (b) 30°.

In Figs. 6 and 7, only the peak point on the main beam and the first two nulls on either side of the main beam are constrained. Although the mean square error (MSE) is greater than the unconstrained LPCM as expected, the main lobe to null difference is better preserved in LC-LPCM and QC-LPCM.

### C. Null depth comparison

The nulls approaching capability of the above-mentioned techniques are compared in Table 1. For broadside pattern, null at 30° and for steered main beam null at 0° has been considered for comparison and the desired null depth is assumed to be -60dB. Both LC-LPCM and QC-LPCM give the best null recovery and are better than UC-LPCM, especially for greater distortion levels.

### D. Interpolation of patterns

In order to show the effect of interpolation, a case is considered in which radiation pattern for bend-angle $\Upsilon = 18°$ is recovered through the interpolation of pre-

stored individual element patterns in Fig. 3. $\Delta\Upsilon = 15°$ together with cubic interpolation is compared with UC-LPCM in Fig. 8 for pattern recovery. One can see that there is not much difference between compensated radiation patterns obtained from accurate pre-stored individual antenna patterns at 18° and the interpolated patterns. So interpolation can be used to reduce the storage data requirements of the proposed algorithm. However, the spacing between the bend angles $\Delta\Upsilon$ needs to be kept within a reasonable range for interpolation to be reliable, as the results deteriorate greatly if $\Delta\Upsilon > 10°$.

Table 1: Null depth comparison of pattern recovery techniques

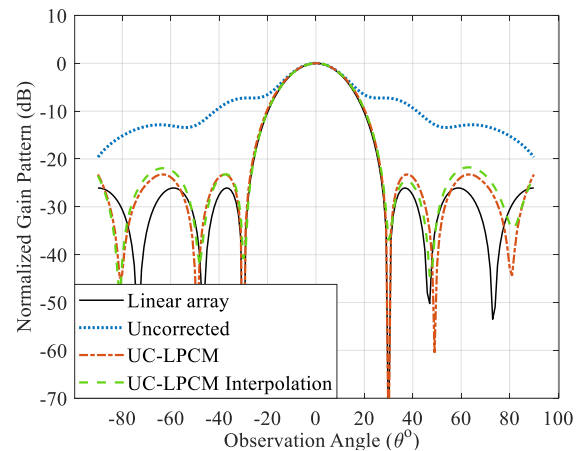| Technique | Broadside | | Main Beam at 30° | |
|---|---|---|---|---|
| | $\Upsilon = 15°$ | $\Upsilon = 30°$ | $\Upsilon = 15°$ | $\Upsilon = 30°$ |
| OCVM | -24dB | -15dB | -17dB | -13dB |
| UC-LPCM | -53dB | -34dB | -40 dB | -27 dB |
| LC-LPCM | -60dB | -60dB | -60dB | -60dB |
| QC-LPCM | -55dB | -51dB | -55dB | -52dB |



Fig. 8. Effect of interpolation for 18° wedge deformed dipole array.

## V. GENERAL DISCUSSION

OCVM method is employed for the compensation of MC and the effect of surface deformity on the array radiation pattern. It is shown that only a partial broadside radiation patterns recovery is obtained, and the results for steered main-beam in directions away from broadside are not good at all. This is because the impedance matrix does not accurately model the effect of MC and deformation and the problem compounds away from the broadside.

Unconstrained linear pattern correction through least square error (LSE) was also used to recover the original pattern of the conformal wedge array. Although pattern recovery was very accurate with the lowest MSE between the desired and compensated radiation patterns, there is little control on the position and depth of the

nulls. As a result, the nulls are partially filled up (-40dB for broadside main-beam pattern) and displaced from the required value by a few degrees. This is one of the simplest methods to recover the desired array pattern with analytical closed-form expressions for calculating the compensated weights.

In order to achieve the maximum recovery at some points in patterns (such as nulls and side-lobe level points), LC-LPCM is investigated. Although the result is promising at constraint points, the algorithm exhibits no control at other points resulting in larger side-lobe levels. This behaviour is because of the search space becoming very limited with a small number of permissible solutions. QC-LPCM gives a better compromise by increasing the search space to hyper-surfaces formed by the constraints. Not only the nulls are recovered while maintaining a low side-lobe level, but a healthy gap between the main lobe and nulls is also obtained.

Since the proposed methods require pre-stored individual element radiation pattern to be available, the effect of pattern interpolation is also investigated in order to reduce the storage cost. It is shown that by using an appropriate bend-angle spacing as pre-stored interpolation points, radiation pattern could be recovered at any arbitrary bend angle with only a marginal performance loss.

## VI. CONCLUSION

From the above discussion, one can conclude that patterns can be recovered for wedge-shaped deformation of antenna arrays at large flex angles (up to 30°) using the constrained LPCM techniques. The proposed techniques only require prior knowledge of individual element patterns of desired and deformed arrays and can be used for different types of resonators. It is shown that the proposed QC-LPCM and LC-LPCM algorithm had an increased peak to null power-ratio without unduly degrading the LSE. It was also shown that a few pre-stored individual antenna patterns can be used to give the desired pattern at any arbitrary bend-angle through interpolation.

## ACKNOWLEDGEMENT

## REFERENCES

[1] P. Chen, Y. Zhao, and C. Liu, "A novel adaptive wideband frequency invariant beamforming algorithm for conformal arrays," *18th International Radar Symposium (IRS)*, Prague, Czech Republic, pp. 1-10, Aug. 2017.

[2] L. Josefsson and P. Persson, *Conformal Array Antenna Theory and Design*. Wiley-IEEE Press, chapter-1, 2006.

[3] B. D. Braaten, S. Roy, S. Nariyal, M. A. Aziz, N. F. Chamberlain, Irfanullah, M. T. Reich, and D. E. Anagnostou, "A self-adapting flexible (SELFLEX) antenna array for changing conformal surface applications," *IEEE Transactions on Antennas and Propagation*, vol. 61, no. 2, pp. 655-665, Feb. 2013.

[4] J.-L. Guo and J.-Y. Li, "Pattern synthesis of conformal array antenna in the presence of platform using differential evolution algorithm," *IEEE Transactions on Antennas and Propagation*, vol. 57, no. 9, pp. 2615-2621, Sept. 2009.

[5] M. A. Aziz, S. Roy, L. A. Berge, Irfanullah, S. Nariyal, and B. D. Braaten, "A conformal CPW folded slot antenna array printed on a Kapton substrate," *6th European Conference on Antennas and Propagation (EUCAP)*, Prague, Czech Republic, pp. 159-162, Mar. 2012.

[6] R. C. Hansen, *Phased Array Antennas*. 2nd edition, John Wiley and Sons, Inc., New York, NY, chapter-7, 2009.

[7] C. A. Balanis, *Antenna Theory: Analysis and Design.* 4th edition, John Wiley & Sons, chapter-16, 2016.

[8] W. L. Stutzman and G. A. Thiele, *Antenna Theory and Design*. 3rd edition, John Wiley & Sons, chapter-8, 2012.

[9] I. J. Gupta and A. A. Ksienski, "Effect of mutual coupling on the performance of adaptive arrays," *IEEE Transactions on Antennas and Propagation*, vol. 31, no. 5, pp. 785-791, Sept. 1983.

[10] A. Tariq, M. Ayaz, W. Saif, S. Khattak, J. Kazim, Irfan ullah, and R. A. Bhatti, "LSE based radiation pattern compensation in wedge shaped deformed conformal antenna arrays," presented in *International Applied Computational Electromagnetics Society (ACES) Symposium*, Beijing, China, July 29-Aug. 1, 2018.

[11] H. T. Hui, M. E. Bialkowski, and H. S. Lui, "Mutual coupling in antenna arrays," *International Journal of Antennas and Propagation*, vol. 2010, 2 pages, 2010.

[12] P. Chakravorty and D. Mandal, "Radiation pattern correction in mutually coupled antenna arrays using parametric assimilation technique," *IEEE Transactions on Antennas and Propagation*, vol. 64, no. 9, pp. 4092-4095, Sept. 2016.

[13] P. Kumari, B. Chauhan, and S. Vijay, "Performance analysis of microstrip conformal antenna array and effect of mutual coupling for different curvature," *International Journal of Computer Applications*, vol. 135, no. 9, pp. 30-35, Feb. 2016.

[14] J. Nasir, M. H. Jamaluddin, M. R. Kamarudin, Irfanullah, Y.-C. Lo, and R. Selvaraju, "A four-element linear dielectric resonator antenna array for beamforming applications with compensation

of mutual coupling," *IEEE Access*, vol. 4, pp. 6427-6437, Oct. 2016.

[15] S. Lou, W. Wang, H. Bao, N. Hu, G. Ge, X. Hu, S. Qian, and C. Ge, "A compensation method for deformed array antennas considering mutual coupling effect," *IEEE Antennas and Wireless Propagation Letters*, vol. 17, no. 10, pp. 1900-1904, Oct. 2018.

[16] A. Tariq, Irfanullah, J. Kazim, M. Ayaz, A. Zaib, R. A. Bhatti, and S. Khattak, "Interpolation based radiation pattern correction in conformal beamforming arrays," *2nd World Symposium on Communication Engineering (WSCE)*, Nagoya, Japan, pp. 102-106, Dec. 2019.

[17] B. Ijaz, A. Sanyal, A. M-Radal, S. Roy, Irfanullah, M. T. Reich, D. Dawn, B. D. Braaten, N. F. Chamberlain, and D. E. Anagnostou, "Gain limits of phase compensated conformal antenna arrays on non-conducting spherical surfaces using the projection method," *IEEE International Conference on Wireless for Space and Extreme Environments*, pp. 1-6, Nov. 2013.

[18] G. Gordon and R. Tibshirani, *Karush-Kuhn-Tucker Conditions, Optimization*, 10-725/36-725, 2012.